# Influence of the Substrate on Order and Image Contrast for Physisorbed, Self-Assembled Molecular Monolayers: STM Studies of Functionalized Hydrocarbons on Graphite and $MoS_2$

**Leanna C. Giancarlo, Hongbin Fang, Seth M. Rubin, Alexa Avila Bront, and George W. Flynn***

*Department of Chemistry and Columbia Radiation Laboratory, Columbia University, New York, New York 10027*

*Received: June 30, 1998; In Final Form: September 11, 1998*

Scanning tunneling microscopy (STM) has been used to investigate the influence of different substrates on monolayer ordering and molecular image contrast for singly and doubly substituted long-chain hydrocarbons. Self-assembly at the phenyloctane−graphite and phenyloctane−$MoS_2$ interfaces can be mildly or strongly affected by the underlying surface. In the most extreme cases, changes in the ordering of two-dimensional adlayers involve both rotation and translation of the molecules. Differences in the electronic characteristics of the underlying surface also have important implications for the STM image contrast exhibited by many molecules. Careful inspection of functional group contrast on both substrates provides useful information about the relative importance of geometric/topological versus electronic coupling factors in the STM tunneling mechanism for physisorbed molecules.

## 1. Introduction

The influence of substrates on molecular ordering at interfaces is one of the crucial issues facing applications of self-assembly techniques to microelectronics and biosensor development. Control of self-assembly has far-reaching implications for tailoring thin-film structures and their resulting properties or functions. Scanning probe microscopies, in particular scanning tunneling microscopy (STM), are well-suited to examine the role of the substrate in thin-film development, especially with regard to separating the effects of adsorbate−adsorbate and adsorbate−substrate interactions. With its ability to attain molecular and in many cases atomic resolution, STM is an extremely sensitive probe for deducing both long-range and local order in physisorbed systems.[1−3] Recently, a number of studies have made use of STM to ascertain the effect of different surfaces on the ordering of molecular assemblies. Some of these investigations demonstrate few if any changes in the organization of the molecular adlayer on different surfaces. For instance, naphthalene-1,4,5,8-tetracarboxylic-dianhydride,[4] perylene-3,4,9,10-tetracarboxylic-dianhydride and -diimide,[5] thioindigo, and tetrachlorothioindigo[6] form similar two-dimensional arrays when adsorbed on both graphite and $MoS_2$; copper phthalocyanine adopts a close-packed structure when epitaxially deposited on graphite and exhibits both close-packed and rowlike forms on $MoS_2$.[7] Other studies have revealed significant modifications of the adsorbate structure in order to register more favorably with the surface features on different substrates. Copper tetra[3,5 di-*tert*-butylphenyl]porphyrin has been found to "contort" when placed on metal surfaces in order to match some property of the substrate lattice.[8,9] Dissimilar adsorbate structures have also been reported for 5,10,15,29-tetrakis(*N*-methylpyridinium-4-yl)-21H,23H-porphine adlayers on iodine-modified Au and Ag surfaces.[10] In addition, dotriacontane molecules align in lamellar fashion with a 60° angle between their long hydrocarbon backbones and the lamella direction on transition-metal dichalcogenides ($MoS_2$, $MoSe_2$), while this same angle is measured as 90° for these molecules on graphite.[11]

In addition to providing information on two-dimensional assembly at interfaces, STM investigations of identical molecules on different conductive or semiconductive surfaces yield crucial information concerning the STM tunneling mechanism. In particular, contributions to the tunneling mechanism made by geometric/topological and electronic coupling factors can be gleaned from probes of the STM contrast for weakly adsorbed molecules on different surfaces. For instance, the tunneling mechanism for molecules containing "chemical marker" groups, functional groups that exhibit significantly increased or decreased image contrast (increased or decreased electron-tunneling probability, respectively), can be expected to be only weakly perturbed between surfaces if tunneling is governed by an "antenna (geometric) effect". This effect presumes that the wave function of the functionalized portion of the molecule extends above both the surface and the rest of the adsorbate allowing it to act as an "antenna" for the tunneling electrons; molecules demonstrating this effect generally have imaging mechanisms governed by molecule-specific topological/geometric factors, which are not expected to be heavily influenced by the substrate. In contrast, molecules whose tunneling mechanism is dominated by electronic factors may be more strongly affected by a change in surface−adsorbate coupling from one substrate to another, particularly in cases where the electronic features of the surface (energy levels, band structure) are substantially altered (e.g. physisorption on a metal compared to a semiconductor).

In this paper, we describe an STM investigation undertaken at the liquid−solid interface that seeks to elucidate the effects of the substrate on (1) the ordering of two-dimensional assemblies of mono- and disubstituted hydrocarbons and (2) the image contrast of chemical markers. Long-chain hydrocarbons containing −S−, OH, COOH, Br, C═C, and $CONH_2$ function-

10.1021/jp982840u CCC: $15.00 
Published on Web 11/19/1998

alities are examined on both semimetallic graphite and semiconductive molybdenum disulfide substrates. Changes in the thin-film organization (ordering) and molecular image contrast have been explored by careful analysis of the STM topographs and are discussed in terms of both the structural (e.g., lattice constants) and electronic (e.g., energetic) properties of the underlying surface.

## 2. Experimental Section

All of the studies described here have been performed using a Nanoscope III scanning tunneling microscope (Digital Instruments) operating at the liquid−solid interface under ambient conditions. Experiments are conducted by immersing an STM tip, mechanically fabricated from 0.25 mm diameter platinum/rhodium (87/13) wire (Omega), into a droplet containing the adsorbate of interest. This liquid droplet consists of a functionalized hydrocarbon dissolved in phenyloctane solution, which is applied directly to the surface of either highly oriented pyrolytic graphite, HOPG (Advanced Ceramics, ZYB grade), or molybdenum disulfide (Ward's Natural Science Establishment). These substrates are freshly cleaved prior to imaging.

Solutions have been prepared by adding between 1 and 40 mg of octadecanamide ($CH_3(CH_2)_{16}CONH_2$), *trans*-9-octadecenoic acid (also referred to as elaidic acid, $CH_3(CH_2)_7CH{=}CH(CH_2)_7COOH$), 11-bromoundecanol ($Br(CH_2)_{11}OH$), 12-bromododecanol ($Br(CH_2)_{12}OH$), 12-bromododecanoic acid ($Br(CH_2)_{11}COOH$), all purchased from Aldrich, or octadecyl sulfide ($CH_3(CH_2)_{17}S(CH_2)_{17}CH_3$), synthesized as in ref 12, to 1 mL of phenyloctane; the quantity of solute depended on the conditions necessary to achieve near saturation of the solutions. The samples were left to dissolve and thermally equilibrate for approximately 24 h prior to usage in the microscope.

With a single exception, the images displayed have been collected in the constant current mode of operation in which the height of the STM tip is readjusted in order to maintain a fixed value for the tunneling current. This results in topographic maps of the adsorbates at the liquid−solid interface where "brighter" portions correspond to topographically higher regions. Setpoint currents in the range 200−800 pA were typically used to obtain molecularly resolved images. For adsorbates on graphite, bias voltages $|V_{bias}| = 0.9-1.5$ V have been used, while for these same molecules deposited on $MoS_2$, the sample bias typically ranged from +1.0−5.0 V. Here, positive voltages indicate tunneling from the tip to the sample, while negative voltages indicate the reverse. All of the images exhibited in the figures are representative of the larger collection of data, and no filtering process has been used to display these data. A zeroth order flattening procedure has been employed, however, to normalize the vertical offset. The metrics noted in the text (molecular length, angles, etc.) are the average of many such measurements using section and/or topview analysis acquired from data sets from numerous, different STM scans; errors in these measurements are typically ±0.05 nm for distances and ±5° for angles.

## 3. Results

**Octadecyl Sulfide.** Octadecyl sulfide, $CH_3(CH_2)_{17}S(CH_2)_{17}CH_3$, forms highly ordered monolayers when physisorbed on $MoS_2$. STM images, like the $10 \times 10$ nm$^2$ constant current one displayed in Figure 1a, reveal well-ordered lamellae separated by dark troughs. Each lamella consists of molecules, represented by the black bar in the figure, possessing centers with heightened contrast. These "bright" regions (areas of greater tunneling probability designated by the arrow in the figure) correspond to the locations of the central S atoms. The alkyl arms extend linearly from the sulfur functionality, yielding a molecular length of 4.38 nm. This value agrees well with that calculated for an all-trans molecule with 36 carbon atoms, where the spacing between alternate carbons is 0.251 nm. The distance between adjacent molecules within a single lamella is measured as 0.48 nm, and the angle between the molecular axis and the lamella direction is approximately 90°.

As described previously and depicted in Figure 1b, octadecyl sulfide forms similar two-dimensional arrays when imaged at the phenyloctane−graphite interface. Again, bright areas demarcate the sulfur functional groups and reflect higher tunneling currents in the vicinity of these atoms. The alkyl chains are aligned along a straight line, as was seen for sulfides adsorbed on $MoS_2$. A comparison of the molecular length, the long molecular axis to lamella angle, and the spacing between molecules within a lamella indicates little if any difference in the self-assembly of this molecule on the semiconductor and semimetal surfaces. A distinction is visible, however, in the STM image contrast exhibited at the position of the sulfur atom relative to the overall contrast along the hydrocarbon chain for this adsorbate on $MoS_2$ and HOPG. When octadecyl sulfide physisorbs on $MoS_2$, the sulfur appears 1.7 times as high as the hydrocarbon arms; on graphite, the relative topographic height is over 2 times as great. One should note that there is a slight voltage dependence for the relative tunneling probability ("brightness") of this sulfide on graphite for bias voltages ranging between +0.6 and +1.6 V;[13] on $MoS_2$ the relative measured topographic height of the S atom (ratio of the normalized height of the functional group to the normalized height of the hydrocarbon chain) is independent of bias, measured in the range +1.6−2.2 V. This difference in functional group contrast for the same molecule on these two substrates is suggestive of a change in the electronic coupling between the molecular adsorbate and these electronically distinct surfaces, as discussed in greater detail below.

**Elaidic Acid.** STM images of elaidic acid, $CH_3(CH_2)_7CH{=}CH(CH_2)_7COOH$, physisorbed on $MoS_2$ also display a high degree of two-dimensional order. As seen in Figure 1c, distinct lamellae are observed on the surface, separated by dark troughs, with each molecule (indicated by a black bar) adopting an all-trans configuration. One molecule is comprised of three parts: a dark trough, bright lines, and a slightly brighter central portion. By comparison with other studies of carboxylic acids using STM,[14−17] we attribute the dark troughs to the locations of the hydrogen-bonding carboxyl groups. The central portion of the molecule is assigned as the position of those carbon atoms involved in the double bond (marked by an arrow in the figure). The remainder of the hydrocarbon chain is designated as the bright lines extending in either direction from the central double-bonded carbons. The measured length of one molecule is 2.55 nm, with a molecule-to-molecule spacing of 0.53 nm. The angle between the long molecular axis and the lamella direction is approximately 94°. It is unclear from the images obtained on $MoS_2$ whether the molecules of elaidic acid align in a "columnar" fashion (within one lamella all of the COOH groups are aligned in a single column) or in an "interdigitating" pattern (within the lamella the COOH groups alternate with $CH_3$ groups in a single column).

Elaidic acid has also been studied in two-dimensional arrays adsorbed on the basal plane of a graphite substrate. A typical $10 \times 10$ nm$^2$ STM image is shown in Figure 1d. As noted by Hatta et al.,[17] this conjugated acid is oriented in an interdigitating form with the carboxylic acid groups of each hydrogen-bonding dimer lying in the dark trough. Again, the carbon atoms of the

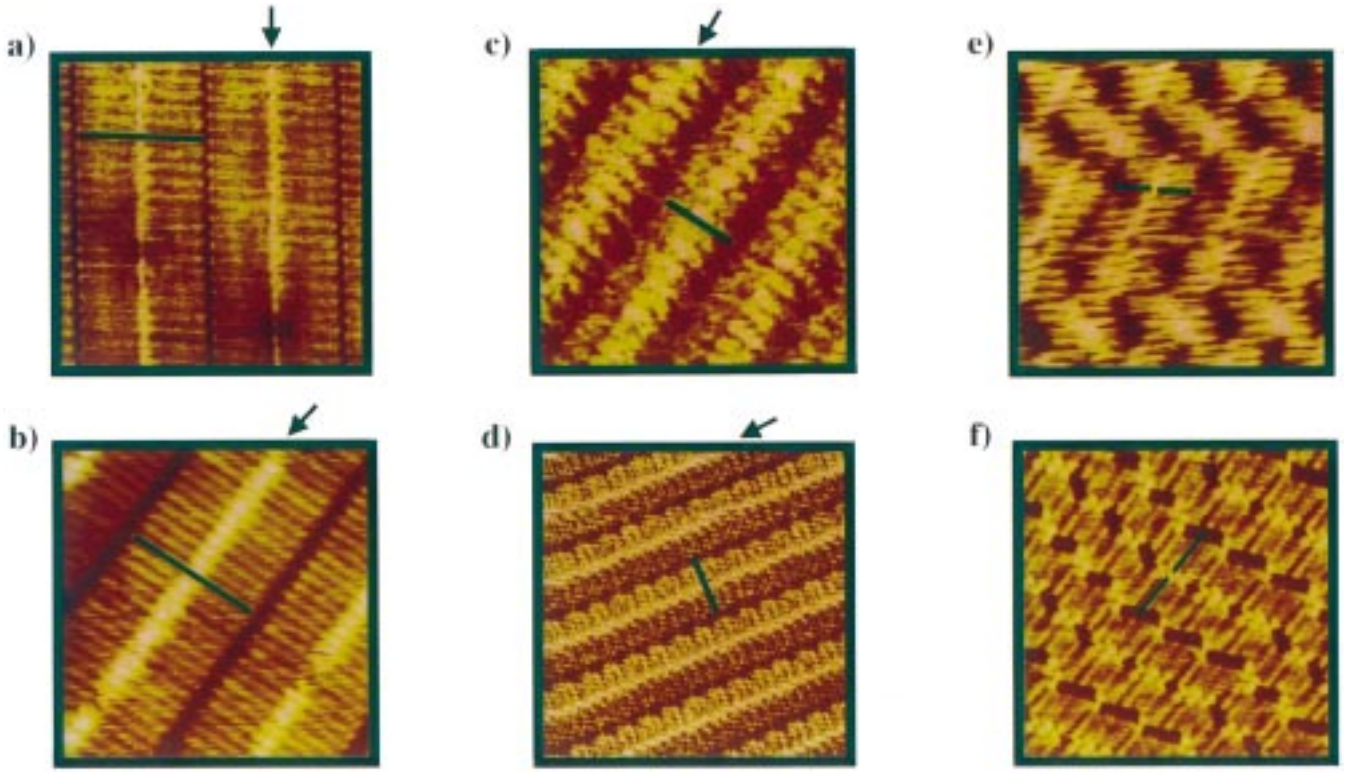


**Figure 1.** STM constant current topographs for octadecyl sulfide, elaidic acid and bromododecanoic acid monolayers. In (a) octadecyl sulfide, $CH_3(CH_2)_{17}S(CH_2)_{17}CH_3$, is imaged at the phenyloctane−$MoS_2$ interface with +1.7 V applied bias and 300 pA setpoint tunneling current. Two lamellae are revealed in this 10 × 10 nm$^2$ image where the length of one molecule (black bar) is shown. The bright spots in the center of the molecule, indicated with the arrow, are areas of increased tunneling probability ascribed to the locations of the sulfur functional group. The 10 × 10 nm$^2$ STM image displayed in (b) shows octadecyl sulfide physisorbed on a graphite substrate at +900 mV bias voltage and 240 pA setpoint current. Again, the bright areas demarcated with an arrow are assigned to the positions of the sulfur atoms along the hydrocarbon chain (black bar). (c) 10 × 10 nm$^2$ constant height image of elaidic acid ($CH_3(CH_2)_7CH{=}CH(CH_2)_7COOH$) molecules assembled on $MoS_2$. Tunneling parameters are +3.0 V bias and 800 pA setpoint current. One molecular length of elaidic acid has been highlighted using the black bar. The carbon−carbon double bond gives rise to increased contrast enhancement in the image (arrow). The constant current topograph of elaidic acid on graphite displayed in (d) has been collected at −1.0 V and 800 pA tunneling current. Again, the arrow guides the eye toward the location of the carbon atoms involved in the double bond. The black bar indicates one molecule adopting an all-trans configuration on the surface. The 12 × 12 nm$^2$ constant current image of 12-bromododecanoic acid, $Br(CH_2)_{11}COOH$, displayed in (e) shows the acid molecules self-assembled on a $MoS_2$ substrate. Tunneling parameters for this image are +5.0 V bias and 300 pA setpoint current. The black bars in the image indicate two molecules arranged in a bromine-to-bromine, head-to-head dimer. The STM topograph in (f) reveals physisorption of bromododecanoic acid on a 12 × 12 nm$^2$ portion of the basal plane of graphite. Typical tunneling conditions are −1.4 V bias and 300 pA setpoint current. As in (e), the bars denote two acid molecules constituting a dimer pair.

double bond appear with greater contrast enhancement than the carboxylic and alkyl arms extending outward from them. A comparison between this molecule on graphite and $MoS_2$ surfaces suggests no changes in the molecular assembly, although the images on $MoS_2$ lack the resolution necessary to establish a definitive assignment as to the packing order. Further, the molecular length, molecule-to-molecule spacing, and molecular axis to lamella angle for elaidic acid on $MoS_2$ are in accord with those measurements reported previously for physisorption on graphite.[16,17] The relative contrast exhibited at the location of the chemical marker group (the double bond) on both substrates is nearly equal with the ratio of the measured relative topographic heights (double bond relative to the hydrocarbon chain) being approximately 1.5. This value is unchanged for a number of bias voltages (−1.0 to −1.6 V) for studies conducted using graphite as the substrate, implying that the imaging mechanism for this molecule is likely dominated by geometric/topological rather than electronic coupling factors.

**Bromododecanoic Acid.** In contrast to elaidic acid and many of the other carboxylic acids studied,[14−17] thin films of 12-bromododecanoic acid, $Br(CH_2)_{11}COOH$, imaged at the phenyloctane−$MoS_2$ interface lack long-range, lamellar order. Instead, as shown in the 10 × 10 nm$^2$ constant current topograph of Figure 1e, only local ordering is observed running in a direction parallel but not perpendicular to the long molecular axis. Here, the black bars in the figure represent a pair of molecules arranged in a head-to-head pattern such that the bromine terminal groups of adjacent molecules lie next to one another. Like elaidic acid, STM images of bromododecanoic acid consist of an area of very great image contrast, a line of less substantial contrast, and a dark spot. These portions are identified as the terminal bromine atom, the hydrocarbon chain, and the carboxyl group, respectively. Each acid group hydrogen bonds to an adjacent carboxyl group. The measured length of one lamella (comprised of two molecules, black bars in Figure 1e) is 3.24 nm. The angle between the direction of the long molecular axis and the trough is approximately 115°.

12-Bromododecanoic acid forms similar self-assemblies when deposited on graphite substrates. A 10 × 10 nm$^2$ topograph is depicted in Figure 1f. Although long-range, lamellar ordering is absent, these brominated acids also organize on graphite in a direction parallel to their long molecular axes. Pairs of molecules in which the bromine atoms are aligned head-to-head are observed alone or in groups of two or three in a direction perpendicular to the long molecular axis.[18] This differs from the interfacial films arranged on $MoS_2$, where as many as six

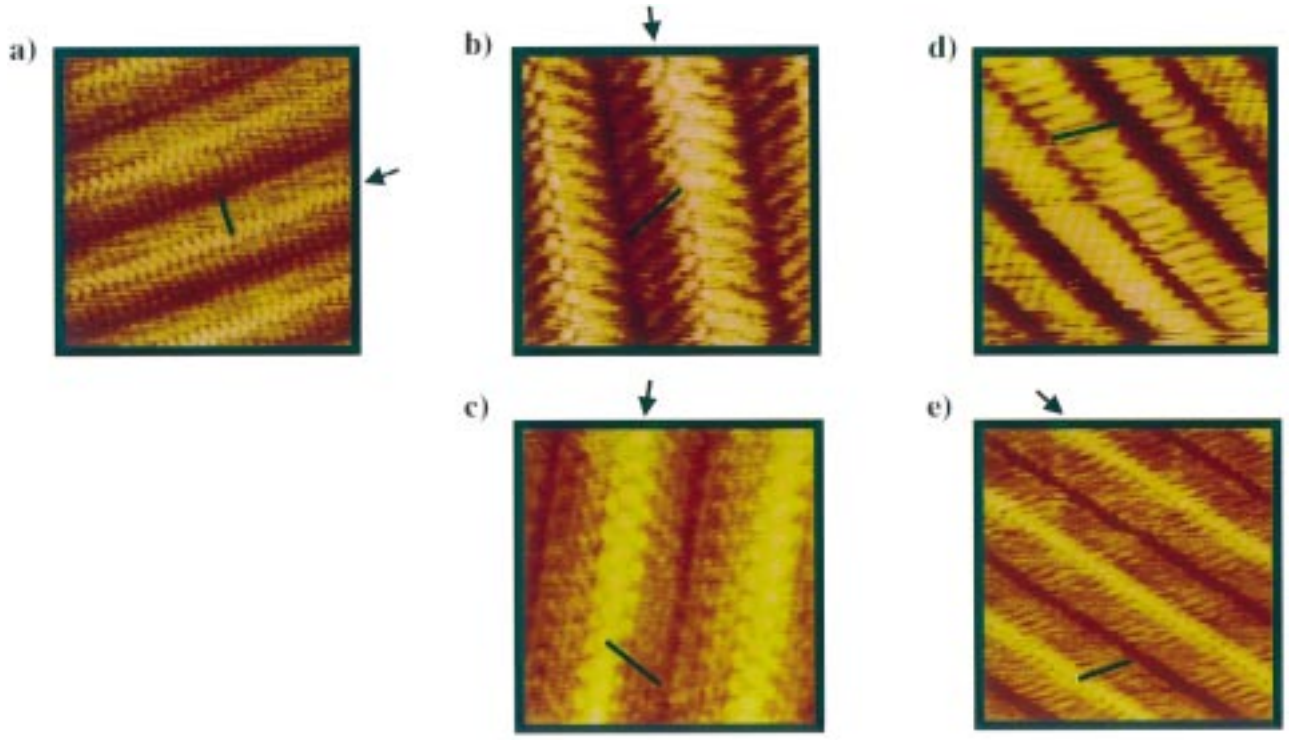


**Figure 2.** Constant current STM images of 12-bromododecanol, 11-bromoundecanol, and octadecanamide. (a) Bromododecanol, $Br(CH_2)_{12}OH$, imaged at the phenyloctane−$MoS_2$ interface with +1.0 V bias and 500 pA setpoint current. The black bar in the 12 × 12 $nm^2$ topograph represents one molecule adopting an all trans configuration on the surface. The brighter spots, indicated with an arrow, are ascribed to the locations of the terminal bromine atoms. A 6 × 6 $nm^2$ image of 11-bromoundecanol, $Br(CH_2)_{11}OH$, adsorbed on $MoS_2$ is shown in (b). The black bar reveals one molecule, while the arrow points to the positions of the bromine atoms. This topograph has been obtained at +900 mV bias voltage and 523 pA setpoint current. The 6 × 6 $nm^2$ image shown in (c) for this same molecule on graphite has been acquired at −1.4 V and 300 pA. (d) 10 × 10 $nm^2$ constant current STM images of octadecanamide, $CH_2(CH_2)_{16}CONH_2$, adsorbed on $MoS_2$. One molecular length is indicated by the black bar. Tunneling conditions are +1.4 V bias and 300 pA setpoint current. The tunneling conditions for octadecanamide physisorbed on the basal plane of graphite, as shown in (e), are +1.4 V bias and 240 pA setpoint. The arrow points to a strip of high tunneling probability assigned as the location of the amide functional groups. Again, the black bar represents the length of one molecule.

head-to-head pairs are found grouped together. Measurements of the length of the molecular axis and the angle between the axis and the trough are consistent with those noted above for physisorption on $MoS_2$. Further, similar image contrast is exhibited by this molecule regardless of the substrate. The resolution of the STM images collected for bromododecanoic acid on graphite and $MoS_2$ differs significantly, however, with atomic resolution achieved for thin films packed on graphite (note the small spots attributable to hydrogen atoms protruding up along the hydrocarbon backbone) but only molecular resolution attainable on $MoS_2$. This difference in image clarity may have its origin in the strength of the adsorbate−adsorbate versus adsorbate−substrate interactions, as discussed below.

**Bromododecanol.** Unlike 12-bromododecanoic acid, 12-bromododecanol, $Br(CH_2)_{12}OH$, assembles in two dimensions such that lamellar order exists at the interface between phenyloctane and $MoS_2$. For large scan sizes (approximately 100 × 100 $nm^2$) not shown here, a single domain of ordered molecules is typically observed. Smaller scanned regions reveal molecules arranged in distinct rows separated by dark troughs. Such an area is displayed in the 12 × 12 $nm^2$ STM topograph of Figure 2a. One molecular length is marked by a black bar and corresponds to a length of 1.86 nm. The angle between the long molecular axis and the lamella direction is 93°. This value differs greatly from the same angle measured for other unsubstituted and monosubstituted alcohols physisorbed on graphite; in these cases, acute angles approaching 60° have been reported.[1,19−22] The lamellar molecule-to-molecule spacing for bromododecanol on $MoS_2$ is 0.45 nm. Like the brominated acids described above and elsewhere,[18,23] each bromododecanol molecule appears with three distinct parts in the STM images. The dark troughs are attributed to the hydrogen-bonding OH groups by comparison with recent work on substituted alcohols.[19] The somewhat "bright" lines lying perpendicular to the trough are assigned as the aliphatic chains with the relatively "brighter" spots (arrow in Figure 2a) designated as the bromine functionalities. Again, the bromine of one molecular adsorbate is arranged head-to-head with the bromine of the adjacent molecule such that these two brominated alcohols constitute a single row within the lamella. The bromine end group appears with a measured topographic height of 1.8 relative to the hydrocarbon chain.

The images of 12-bromododecanol on graphite, described in detail elsewhere,[19] differ in two respects from topographs obtained here using $MoS_2$ as the substrate. First, although this brominated alcohol forms well-ordered arrays at the liquid−graphite interface (the metrics, measured spacings, and molecular lengths for this molecule on both substrates are very similar), these assemblies are characterized by a "herringbone" pattern on graphite arising from approximately 60° angles between the long axis of the molecule and the direction of the lamellae. This angle results from the strong hydrogen bonding between adjacent adsorbate molecules. The herringbone pattern has not been observed for bromododecanol physisorbed on $MoS_2$. Second, only "dark" bromine conformers have been detected when 12-bromododecanol is imaged on graphite.[19] (Here, "dark" refers to the relative contrast between the Br functional group and the remainder of the molecule and signifies lower tunneling probability.) This observation differs both from those for monolayers of this molecule on $MoS_2$ and from those

of other brominated molecules on graphite.[1,18,20,23] For instance, both "bright" and "dark" bromine configurations have been reported for 1-bromodocosane ($CH_3(CH_2)_{21}Br$) imaged at the phenyloctane−graphite interface.[1,20] The transition between these two conformations has been presumed to arise from the rotation of the Br end group from a position within the plane of molecules lying on the surface (all-trans molecular configuration assigned as leading to "dark" bromine images) to a position above the plane of molecules (gauche conformation resulting in "bright" bromines, implying an "antenna effect").

**Bromoundecanol.** 11-Bromoundecanol, $Br(CH_2)_{11}OH$, assembles in well-ordered adlayers when deposited on $MoS_2$ substrates. As seen in the $6 \times 6$ nm$^2$ topograph of Figure 2b, distinct lamellae of the 11-brominated alcohol appear at the phenyloctane−$MoS_2$ interface. These lamellae are characterized by light and dark columns, each of which indicates the location of one molecule, as represented by the black bar in the figure. One molecular length has been measured as 1.43 nm with a 0.41 nm molecule-to-molecule spacing. Again, the brightest spots in the image (arrow in Figure 2b) represent areas of high electron-tunneling probability and are assigned as the locations of the bromine terminal group. The hydroxyl groups are attributed to the dark troughs. Each single lamella is composed of a pair of bromine molecules lying in a head-to-head configuration. These pairs are arranged in a herringbone pattern and organize with a 56° angle between the long molecular axis and the lamellar direction. As noted above, one 11-bromoundecanol in this pair appears with darker contrast than the other, presumably resulting from poorer registry with the underlying semiconductor lattice.

Two lamellae are also shown in Figure 2c for interfacial thin films of 11-bromoundecanol on graphite. In the STM topograph, one molecule consists of a bright spot (indicated by the arrow) followed by a somewhat dimmer line of spots and a dark trough. The length of a single molecule within the lamella (black bar) is 1.51 nm. This value agrees well with that expected for a hydrocarbon chain of 11 methylene units adopting an all-trans conformation on the surface. These brominated alcohols appear in a herringbone configuration with a 63° angle between the long molecular axis and the lamella direction. On the basis of comparison with other brominated molecules, including those described in detail above, the bright spots in the images are attributed to the positions of the bromine atoms, which are arranged in a head-to-head configuration. The dimmer spots are ascribed to the hydrocarbon chain with the hydrogen-bonding hydroxyl groups residing in the dark trough. The loss in clarity along the hydrocarbon chain, evident in the STM image, may arise from bromoundecanol molecules undergoing rotation about the O−C bond such that the molecules alternate between a herringbone and a parallel pattern on the surface. This interchange between structures is known as a rotator phase and has been reported in studies of the crystalline structures of *n*-alkanes,[24−27] alkenes,[28] and alcohols.[29−31] Rotator phases have also been observed in temperature-dependent STM studies of 1-dodecanol on graphite.[32] It should be mentioned that, in both possible orientations for 11-bromoundecanol, the angle between the molecular axis and the trough will remain unchanged. The presence of alternating structures resulting from a phase transition has not been detected for this brominated alcohol imaged on $MoS_2$.

There are two noticeable differences between the STM images for physisorption of bromoundecanol on $MoS_2$ and the basal plane of graphite. First, the resolution in the images increases substantially when these brominated hydrocarbons are deposited on a graphite substrate as opposed to $MoS_2$. In Figure 2b, "bars of contrast" indicate the direction of the hydrocarbon chain, while in Figure 2c small spots are seen, which may be attributed to individual methylene units. This change in resolution, from molecular to atomic, has also been observed for both elaidic acid and bromododecanoic acid molecules on these same surfaces and may derive from better "meshing" between the molecular backbone and the underlying substrate spacings. (See Discussion below.) Second, a sharp alternation in contrast dominates images of bromoundecanol on $MoS_2$ (Figure 2b); within one lamella half of the molecules appear with very bright contrast (see for example those molecules lying to the right of the arrow shown in the figure), while the others exhibit poor (dark) contrast. This effect is not prevalent in STM topographs of this same molecule on graphite (Figure 2c). Again, one possible explanation for this moiré pattern is an interference arising from a lack of registry between half of the molecules within one lamella and the semiconductor surface. STM images of the $MoS_2$ surface acquired after the collection of the topograph displayed in Figure 2b (obtained by changing the electron-tunneling parameters so that only the underlying $MoS_2$ can be seen) reveal poorer registry between the molecules that appear dark and the atoms of the substrate than the molecules that appear bright and the substrate atoms.

**Octadecanamide.** As shown in Figure 2d, octadecanamide, $CH_3(CH_2)_{16}CONH_2$, forms ordered arrays when physisorbed on a $MoS_2$ surface. As displayed in this $10 \times 10$ nm$^2$ constant current topograph, the amide molecules arrange in lamellar fashion with dark troughs separating individual molecules in adjacent lamellae. One molecular length, demarcated by the black bar in the figure, corresponds to 2.37 nm; the molecule to molecule spacing is 0.47 nm. As a result of the decreased STM contrast at both ends of the molecule, the methyl terminal group on one side of the molecule cannot be distinguished from the amide functionality on the other side. As depicted in the STM image and Figure 3, octadecanamide molecules may hydrogen bond to each other in two configurations. In the first, the molecules lie flat on the surface, nearly aligned along the same line (drawn through their long molecular axes); this is designated as the parallel configuration. In the other, molecules orient at approximately a 120° angle with respect to each other, forming a herringbone pattern reminiscent of that observed for short-chain length *n*-alcohols adsorbed on graphite at room temperature and 11-bromoundecanol on $MoS_2$ described above. For both the parallel and herringbone configurations, the angle between the amide long molecular axis and the dark troughs (where the $CONH_2$ groups are located) is approximately 63°.

STM images such as the one portrayed in Figure 2e reveal self-assembled monolayers of octadecanamide on the basal plane of a graphite surface. As reported recently,[33,34] these amide molecules readily physisorb onto HOPG to form domains of molecules aligned along the underlying substrate directions. As shown in Figure 2e, each lamella is comprised of two molecules hydrogen bonded together at the amide functional group. One such molecule is denoted by the black bar superimposed on the STM image. This molecule possesses ends of alternate contrast ("bright" and "dark") connected by a series of small spots. The region of enhanced contrast (high tunneling probability), demarcated by the arrow, has been previously assigned as the location of the hydrogen-bonding amide moiety; the methyl end of octadecanamide lies close to the dark trough with the hydrocarbon backbone in between. The length of the amide molecule on HOPG and the molecule-to-molecule spacing are consistent with the values measured on the $MoS_2$ substrate. Here,

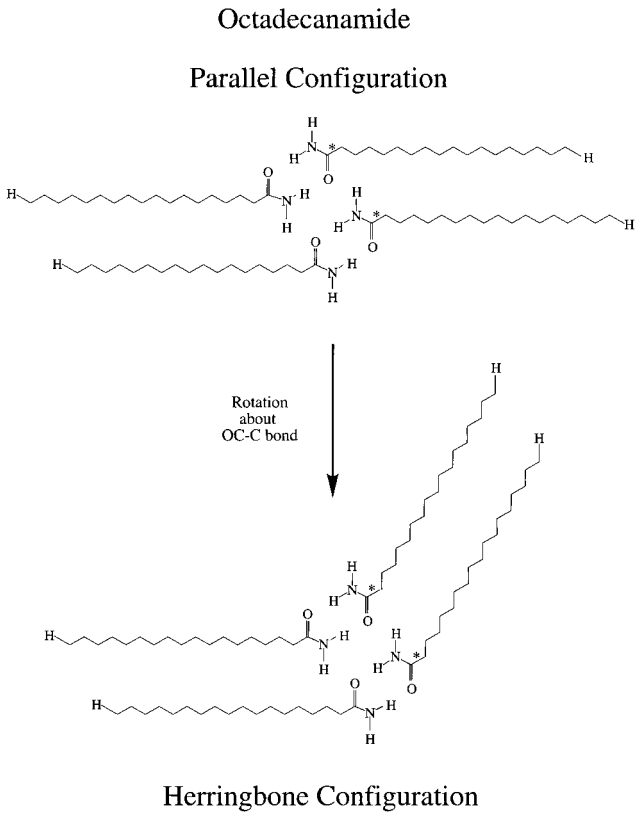


**Figure 3.** Schematic representation of the parallel and herringbone configurations of octadecanamide, $CH_2(CH_2)_{16}CONH_2$, observed on graphite and $MoS_2$ surfaces via STM. Transformation from one configuration to the other may involve rotation about the carbon−carbon bond adjacent to the amide group, marked with the asterisk.

molecules are arranged in a parallel configuration with a long molecular axis to lamella angle of approximately 65°.

Two striking differences are readily apparent in comparing physisorption of octadecanamide on graphite and $MoS_2$. First and most conspicuous, the amide functional group appears with increased contrast, i.e., "brightness" relative to the hydrocarbon chain, when imaged by STM at the phenyloctane−graphite interface but exhibits a decrease in image contrast, i.e., "dark", when examined at the phenyloctane−$MoS_2$ interface. This significant transformation in tunneling probability has implications regarding the STM imaging mechanism for this molecule and points toward a change in electronic coupling between the molecule and the surface as discussed below. The idea that the imaging mechanism for octadecanamide may be dominated by electronic factors (as opposed to geometric/topological effects) is supported by a sharp change in image contrast with applied bias voltage for this amide on HOPG.[13] Second, the long-range packing order changes from one substrate to the other. On the basal plane of graphite, octadecanamide assembles in a parallel configuration, while on $MoS_2$, herringbone patterns are also observed. As in the cases of 11-bromoundecanol and 12-bromododecanol, this variation in packing order may result from differences in the affinities of the molecule for these dissimilar substrates (subtle changes in adsorbate−substrate interactions).

## 4. Discussion

**Effect of the Substrate on Monolayer Order.** As noted above, different surfaces can have dramatic effects on the ordering of monolayers of the same molecules. The similarities and differences in molecular chain length, molecule-to-molecule spacing, and the angle between the long molecular axis and the lamella direction for assembly on $MoS_2$ and graphite are summarized in Table 1. While these two materials are both ideally suited substrates for the study of molecular assembly via STM due to their innate flatness and ease of preparation, the differences between their lattice constants, 0.246 nm for HOPG and 0.316 nm for $MoS_2$, and electronic band structures makes such investigations particularly intriguing.

In general, domains with dimensions of $100 \times 100$ nm$^2$ or larger have been observed for these molecules self-assembled on graphite and $MoS_2$. The assemblies are very reproducible, and all of the monolayers on graphite are stable for times on the order of minutes. On $MoS_2$, the molecular films are less stable, most likely owing to weaker adsorption on the surface, which favors dissolution into the phenyloctane solvent as discussed below.

The manner in which the molecules examined in this STM study organize on these two surfaces can be divided into three categories: similar ordering irrespective of the substrate, slightly modified organization induced by the underlying surface, and a significant change in assembly due to the surface structure. The STM images of monolayers of octadecyl sulfide (Figure 1, parts a and b), elaidic acid (Figure 1, parts c and d), and 11-bromoundecanol (Figure 2, parts b and c) appear very similar on both $MoS_2$ and graphite. The fact that the lengths of the long molecular axes, the distances between molecules, and the angles between the molecular axis and the lamella direction agree well for molecular ordering on both surfaces suggests that adsorbate−adsorbate interactions are slightly more important in molecular assembly than adsorbate−substrate coupling. This contrasts strongly with a report of the ordering of alkylcyanobiphenyls on these two surfaces where the molecule−surface interactions govern self-assembly leading to increased spacings between these liquid-crystal molecules on $MoS_2$ as a result of a larger substrate lattice constant.[35] The major difference between the images of substituted long-chain hydrocarbons on $MoS_2$ and graphite, described above, stems from the resolution achieved in the topographs. For topographs collected where graphite has been used as the substrate, atomic resolution within individual molecules is frequently attained; on $MoS_2$, however, molecular (or, in the best cases, submolecular) resolution is usually the norm. This difference in resolution has also been reported for comparative studies of *n*-alkanes,[11] $C_6Br_6$,[36] and in theoretical calculations for adsorption of $C_6H_6$ on $MoS_2$ and graphite[37] and likely derives from greater mobility of the molecular adsorbates on $MoS_2$. Increased molecular motion is also in accord with lower heats of adsorption measured for many molecules, including paraffins, on $MoS_2$ compared to on graphite; in fact, the heat of adsorption of *n*-dotriacontane on $MoS_2$ was found to be approximately one-third of the value obtained on graphite.[38] Further, decreased strength in adsorbate−substrate interactions may also result in shorter residence times for the molecules on the surface. Equivalently, shorter residence times arise from a shift in the competition between molecules remaining physisorbed on the surface (heat of adsorption) or resolvating in the phenyloctane solution (heat of solvation).

12-Bromododecanoic acid (Figure 1, parts e and f) forms two-dimensional assemblies, which possess nearly the same molecular parameters (lamellar distance, angle, etc.) on both substrates; however, STM images reveal slightly more order in the direction perpendicular to the long molecular axis when self-assembly occurs at the phenyloctane−$MoS_2$ interface. Here, as many as six molecules are arranged together, while a maximum of three bromododecanoic acid molecules group together on graphite.[18]

**TABLE 1: Comparison between Molecular Parameters for Self-Assembly on $MoS_2$ and Graphite**

| | $MoS_2$ | | | Graphite | | |
|---|---|---|---|---|---|---|
| molecule | molecular length (nm)[d] | angle (deg) | spacing between molecules (nm) | molecular length (nm) | angle (deg) | spacing between molecules (nm) |
| octadecyl sulfide | 4.38 | 90 | 0.48 | 4.35 | 99 | 0.43 |
| elaidic acid | 2.55 | 94 | 0.53 | 2.43 | 87 | 0.43 |
| 12-bromododecanoic acid | 3.24[a] | 115 | | 3.70[a] | 117 | 0.42 |
| 12-bromododecanol | 1.86 | 93 | 0.45 | 1.78[b] | | 0.46[b] |
| 11-bromoundecanol | 1.43 | 56 | 0.41 | 1.51 | 63 | 0.49 |
| octadecanamide | 2.37 | 117 | 0.47 | 2.4−2.6[c] | 115−120[c] | 0.48[c] |

[a] Length of two molecules comprising a "dimer" pair. [b] Claypool, C. L.; Faglioni, F.; Goddard, W. A.; Gray, H. B.; Lewis, N. S.; Marcus, R. A. *J. Phys. Chem. B* **1997**, *101*, 5978−5995. [c] Takeuchi, H.; Kawauchi, S.; Ikai, A. *Jpn. J. Appl. Phys.* **1996**, *35*, 3754−3758. [d] Error bars on distances are ±0.05 nm; errors on angles are ±5°.

Again, this disparity in short-range order (long-range order is only present in the images in the direction parallel to the molecule's long axis) likely derives from a variation in the strength of adsorbate−adsorbate versus adsorbate−substrate interactions. Like some of the other molecules mentioned above, monolayers of bromododecanoic acid on $MoS_2$ are generally dominated by the hydrogen-bonding interactions existing between molecules. The substrate is important in providing a flat surface on which this assembly forms but does not act as a strict formation template (unlike the case of the alkylcyanobiphenyls). When physisorbed on graphite, however, the interaction of the acid molecules and the substrate plays a larger (although probably not dominant) role, leading to the prevalence of pairs of molecules (black bars in Figure 1, parts e and f) arranged alone or in groups of two or three on the surface of the substrate.

Likewise, the ordering of octadecanamide adlayers (Figure 2, parts d and e) is found to be controlled by the intermolecular interactions present between the hydrogen-bonding amide functional groups. For assemblies of these molecules, a different packing orientation was observed on $MoS_2$ than on graphite. On the former, some columns of the molecules are organized in a herringbone configuration, while on the latter only a parallel arrangement of molecules has been detected. Again, the strong hydrogen bonding between molecules likely drives assembly in two dimensions and lends stability to the monolayers that are formed; however, it is believed that weaker molecule−surface interactions for physisorption on $MoS_2$ permit rotation about the carbon−carbon bond involving the amide functionality leading to the herringbone pattern as demonstrated in Figure 3. On graphite, the stronger interaction between the long alkyl chain and the "honeycomb" surface makes this rotation unlikely. The streakier image shown in Figure 2d likely results from greater mobility induced by this rotation, which resembles a rotator phase similar to that observed in solid crystals of *n*-alkanes,[24−27] alkenes,[28] and alcohols.[29−31]

12-Bromododecanol (Figure 2a) has the most substantial change in self-assembly on the semiconductor substrate compared to the graphite semimetallic surface. Here, the molecular axis to trough angle opens to approximately 90°, while this same angle measures approximately 60° at the phenyloctane−graphite interface. This dramatic change in molecular organization is reminiscent of the difference in physisorption of *n*-alkanes on $MoS_2$ and $MoSe_2$ versus graphite. In their studies, Cincotti and Rabe[11] found that dotriacontane ($C_{32}H_{66}$) assumed a herringbone configuration when placed upon the semiconductor surfaces. (On graphite, parallel orientations have been observed where the *n*-alkane long molecular axis lies normal to the lamellar direction.)[1,20−22,39−41] In Figure 2a, however, the STM topographs may reveal an adsorbate ordered state resulting from a phase transition involving both rotation about the hydroxylated carbon−carbon bond and translation of the molecules along their long molecular axis. Rotator phases involving both rotational and translational degrees of freedom have been described for *n*-paraffins in both experimental studies and theoretical calculations.[42,43] This motion amounts to a weakening of the hydrogen bond with consequent separation of the molecules facing each other so that the 12-bromododecanol adopts a more "alkane-on-graphite-like" structure on the semiconductor surface. Such a weakening of the hydrogen bond is presumably compensated for by stronger $MoS_2$−adsorbate interactions. Further, the two-dimensional structure of 12-bromododecanol may involve a maximization of the bromine−bromine interactions between nearby molecules. It has been speculated that the combination of these two effects (hydrogen bonding and bromine−bromine interactions) leads to the unique patterns detected via STM for 2-bromohexadecanoic acid on graphite[23] and possibly induces subtle effects in the two-dimensional ordering of other substituted carboxylic acids (e.g., 12-bromododecanoic acid imaged at the phenyloctane−graphite interface).[44]

**Effect of the Substrate on Molecular Image Contrast.** In addition to the changes observed in self-assembly (ordering) of molecules containing S, Br, OH, COOH, $CONH_2$, and C═C functionalities when physisorbed on $MoS_2$ and graphite, the molecular image contrast in STM for several of these molecules is altered. Variations in the STM image contrast for the same molecules applied to different substrates have significant implications regarding the dominant factors in the electron-tunneling mechanism for these weakly adsorbed species. In particular, studies such as these provide important information regarding the interplay between geometric/topological factors and electronic coupling.

It has previously been proposed that electron tunneling for many, long-chain, physisorbed molecules becomes possible when there is a weak electronic coupling between the adsorbate and substrate such that the electronic levels of the adsorbate, which lie far from the surface Fermi level, add (albeit only slightly) to the local density of states at this substrate Fermi level.[1,2,13,19,20,45] More significant is the fact that this additional electron density is pushed away from the surface, localized over the molecule, so that at large distances from the surface electron tunneling via STM becomes more efficient over the molecule than over the surface, i.e., there is greater spatial overlap between the STM tip and the molecule than the tip and the surface (the "antenna" effect). This idea is consistent with the fact that the tunneling probability decays exponentially with distance so that even a weakly coupled adsorbate decreases the space between the tip and the adsorbate-modified substrate, making the molecules "visible" in STM. The atomic analogy is the case of Xe on Ni(110).[46] The image contrast for molecules whose tunneling is governed by this "antenna effect" is not expected to be strongly affected by the nature of the electronic structure

of the substrate and, thus, should appear with similar contrast regardless of the surface onto which they self-assemble.

Those molecules that are more strongly coupled to the substrate, whose electronic levels mix more substantially with the surface Fermi level or whose electronic levels lie within the "conduction region", tend to exhibit resonant tunneling. Here, the "conduction region" refers to that area in energy space defined by the difference between the Fermi levels of the tip and the substrate with and without an applied bias voltage. On the basis of an investigation of the voltage dependence of molecular image contrast,[13] it has been suggested that the STM tunneling for at least one of the molecules included in the current study may involve a "resonant" process, and thus STM images may reveal dramatically altered contrast over the functional group when placed upon a different substrate. This stems from the fact that the electronic nature of the substrates ($MoS_2$ and graphite), themselves, are very different. Graphite is a layered, semimetallic surface dominated by electronic delocalization of the carbon $\pi$ electrons. $MoS_2$, on the other hand, is a semiconductor formed of stacked S−Mo−S layers. Its experimentally derived band structure reveals an energy gap in excess of 1 eV separating the valence and conduction bands;[47] theoretical calculations predict a band gap value of 1.2 eV.[48] The first valence band (which includes the valence band maximum) principally consists of Mo $d_{z^2}$ character orbitals; the lowest lying conduction band is a mixture of both Mo "d" and S "p" orbitals.[47−49] One interesting implication of the electronic band structure of $MoS_2$ is the fact that STM tunneling for molecules adsorbed on this surface usually proceeds in only one direction. In the STM images for assemblies on $MoS_2$ shown in Figures 1 and 2, tunneling occurs from the tip to the substrate in all cases (sample biased positive relative to the tip). This is also the case for $C_6Br_6$[36] and $C_{32}H_{66}$.[11] (It has been noted that STM imaging of molecular adsorbates on graphite proceeds independently of the polarity of the applied bias.) This asymmetry in the polarity of the bias voltage has been attributed to the rectifying behavior of the $MoS_2$ substrate[36] and to the fact that naturally occurring $MoS_2$ is usually p-doped.[35]

STM topographs of molecular arrangements of elaidic acid, 12-bromododecanoic acid, and 11-bromoundecanol (Figure 1, parts c and d, e and f, and b and c, respectively) all exhibit similar molecular image contrast regardless of the substrate. These molecules possess "bright" spots of increased tunneling probability localized over the functionalized portion of the molecule when they are imaged at both the phenyloctane−graphite and phenyloctane−$MoS_2$ interfaces. This suggests that topological/geometric factors dominate in the STM tunneling mechanism for these adlayers. Like Xe/Ni(110),[46] elaidic acid, bromododecanoic acid, and bromoundecanol are only weakly electronically coupled to either flat substrate. The extension of electron density, due to the presence of the molecule (especially over the substituted portion), into the gap between the tip and the substrate increases the electron-tunneling probability over the adsorbate, resulting in visibility in the STM and "bright" spots along the molecular axis. The STM tunneling mechanism for octadecyl sulfide (Figure 1, parts a and b) is also likely driven by geometric considerations; however, the contrast exhibited over the position of the sulfur atom appears to decrease slightly when $MoS_2$ is used as the substrate. This presumably arises from an increase in the electronic coupling (compared to the molecules noted above) between the adsorbate and the surface and is in accord with bias voltage dependent results for the image contrast of this molecule on graphite.[13]

12-Bromododecanol and octadecanamide appear with reverse contrast at the locations attributed to the functional groups (Br and $CONH_2$) when arrayed on $MoS_2$ and graphite (Figure 2, parts a, d, and e, here, and Figure 10 of ref 19). On graphite, the brominated end of bromododecanol appears with darkened contrast relative to the hydrocarbon chain; on $MoS_2$, the bromine atom appears brighter than the carbon backbone. One possible reason for this change in contrast may be very strong electronic coupling between an energy level of the molecular adsorbate and the $MoS_2$ substrate such that a resonant tunneling occurs. This seems unlikely in light of preliminary bias voltage dependence results for the image contrast, which suggest that the contrast over the brominated portion of the molecule is independent of the applied bias. This weakens the possibility that the "bright" contrast results from a fortuitous choice of tunneling parameters in which an adsorbate level lying near to the tip−$MoS_2$ conduction region has been "tuned" into resonance. A second possibility in which the "bright" bromine configuration of bromododecanol has not been sampled in the experiments on graphite may be more likely. Other brominated molecules (e.g., 1-bromodocosane)[1,20] have appeared on graphite with both "bright" and "dark" contrast seen over the bromine atom arising from a rotation of this end group from an all-trans configuration within the molecular plane to a gauche configuration extending above the plane. This rotation can then result in more favorable spatial overlap between the tip and the end group in the gauche configuration leading to "bright" spots. In this case, the tunneling mechanism would again be dominated by geometric/topological, i.e., "antenna", effects. Both these hypotheses await further experimentation and evaluation.

Electronic coupling factors seem to play the largest role in the STM tunneling mechanism for octadecanamide. On graphite, the amide functional group appears with increased contrast, while on $MoS_2$, the contrast is darker than the rest of the molecule. These results would tend to suggest that the electronic energy levels of the adsorbate are perturbed differently in the presence of the two surfaces. On graphite, an octadecanamide energy level appears to move closer to the conduction region leading to a "peak" in the voltage dependence of the molecular image contrast due to a resonance in the STM tunneling process. On $MoS_2$, we speculate that the adsorbate energy levels are pushed farther away from the surface Fermi level leading to decreased contrast. In the absence of strong electronic coupling between the adsorbate and the substrate, the tip is expected to remain at the same distance from the molecule while scanning over it at constant current. On the other hand, the tip might move closer to the molecule over the location of the functional group due to its decreased height (relative to the methylene groups) resulting from hydrogen bonding to its neighbor.

## Conclusions

Scanning tunneling microscopy has been used to investigate the influence of graphite and $MoS_2$ substrates on monolayer ordering and molecular image contrast for mono- and disubstituted long-chain hydrocarbons. For many molecules, self-assembly in two dimensions yields identical or nearly identical patterns in the STM topographs on both surfaces; for other molecules, dramatic changes are revealed that may involve both the rotational and translational degrees of freedom of the adsorbate. The underlying surface also appears to have important consequences for the STM image contrast exhibited by many molecules. Analysis of functional group contrast on both substrates suggests an interplay between geometric/topological and electronic coupling factors in the STM tunneling mechanism.

**Acknowledgment.** The work described here has been supported by the National Science Foundation (DMR-94-24296 and CHE-97-27205) and by the Joint Services Electronics Program (U.S. Army, Navy, and Air Force; DAAG55-97-1-0166). S.M.R. also acknowledges support from the Columbia College Rabi Scholars Program and the V. Kann Rasmussen Foundation.

## References and Notes

(1) Cyr, D. M.; Venkataraman, B.; Flynn, G. W. *Chem. Mater*. **1996**, *8*, 1600−1615.
(2) Giancarlo, L. C.; Flynn, G. W. *Annu. Rev. Phys. Chem.* **1998**, *49*, 297−336.
(3) Ikai, A. *Surf. Sci. Rep.* **1996**, *26*, 261−332.
(4) Strohmaier, R.; Ludwig, C.; Petersen, J.; Gompf, B.; Eisenmenger, W. *Surf. Sci.* **1996**, *351*, 292−302.
(5) Ludwig, C.; Gompf, B.; Petersen, J.; Strohmaier, R.; Eisenmenger, W. *Z. Phys. B: Condens. Matter* **1994**, *93*, 365−373.
(6) Petersen, J.; Strohmaier, R.; Gompf, B.; Eisenmenger, W. *Surf. Sci.* **1997**, *389*, 329−337.
(7) Ludwig, C.; Strohmaier, R.; Petersen, J.; Gompf, B.; Eisenmenger, W. *J. Vac. Sci. Technol. B* **1994**, *12*, 1963−1966.
(8) Jung, T. A.; Schlittler, R. R.; Gimzewski, J. K.; Tang, H.; Joachim, C. *Science* **1996**, *271*, 181−184.
(9) Jung, T. A.; Schlittler, R. R.; Gimzewski, J. K. *Science* **1997**, *386*, 696−698.
(10) Itaya, K.; Batina, N.; Kunitake, M.; Ogaki, K.; Kim, Y.-G.; Wan, L.-J.; Yamada, T. *ACS Symp. Ser.* **1997**, *656*, 171−188.
(11) Cincotti, S.; Rabe, J. P. *Appl. Phys. Lett.* **1993**, *62*, 3531−3533.
(12) Bain, C. D.; Troughton, E. B.; Tao, Y.-T.; Evall, J.; Whitesides, G. M.; Nuzzo, R. G. *J. Am. Chem. Soc.* **1989**, *111*, 321−335.
(13) Giancarlo, L.; Cyr, D.; Muyskens, K.; Flynn, G. W. *Langmuir* **1998**, *14*, 1465−1471.
(14) Stabel, A.; Dasaradhi, L.; O'Hagan, D.; Rabe, J. P. *Langmuir* **1995**, *11*, 1427−1430.
(15) Hibino, M.; Sumi, A.; Hatta, I. *Jpn. J. Appl. Phys.* **1995**, *34*, 3354−3359.
(16) Hibino, M.; Sumi, A.; Hatta, I. *Jpn. J. Appl. Phys.* **1995**, *34*, 610−614.
(17) Hatta, I.; Nishino, J.; Sumi, A.; Hibino, M. *Jpn. J. Appl. Phys.* **1995**, *34*, 3930−3936.
(18) Fang, H.; Giancarlo, L. C.; Flynn, G. W. *J. Phys. Chem. B* **1998**, *102*, 7421−7424.
(19) Claypool, C. L.; Faglioni, F.; Goddard, W. A.; Gray, H. B.; Lewis, N. S.; Marcus, R. A. *J. Phys. Chem. B* **1997**, *101*, 5978−5995.
(20) Cyr, D. M.; Venkataraman, B.; Flynn, G. W.; Black, A.; Whitesides, G. M. *J. Phys. Chem.* **1996**, *100*, 13747−13759.
(21) Venkataraman, B.; Breen, J. J.; Flynn, G. W. *J. Phys. Chem.* **1995**, *99*, 6608−6619.
(22) Venkataraman, B.; Flynn, G. W.; Wilbur, J.; Folkers, J. P.; Whitesides, G. M. *J. Phys. Chem.* **1995**, *99*, 8684−8689.
(23) Fang, H.; Giancarlo, L. C.; Flynn, G. W. *J. Phys. Chem. B* **1998**, *102*, 7311−7315.
(24) Maroncelli, M.; Strauss, H. L.; Snyder, R. G. *J. Chem. Phys.* **1985**, *82*, 2811−2824.
(25) Lévay, B.; Lalovic, M.; Ache, H. J. *J. Chem. Phys.* **1989**, *90*, 3282−3291.
(26) Sirota, E. B.; King, H. E., Jr.; Shao, H. H.; Singer, D. M. *J. Phys. Chem.* **1995**, *99*, 798−804.
(27) Sirota, E. B.; King, H. E., Jr.; Singer, D. M.; Shao, H. H. *J. Chem. Phys.* **1993**, *98*, 5809−5824.
(28) Gang, H.; Gang, O.; Shao, H. H.; Wu, X. Z.; Patel, J.; Hsu, C. S.; Deutsch, M.; Ocko, B. M.; Sirota, E. B. *J. Phys. Chem. B* **1998**, *102*, 2754−2758.
(29) Sirota, E. B.; Wu, X. Z. *J. Chem. Phys.* **1996**, *105*, 7763−7773.
(30) Barton, S. W.; Thomas, B. N.; Flom, E. B.; Rice, S. A.; Lin, B.; Peng, J. B.; Ketterson, J. B.; Dutta, P. *J. Chem. Phys.* **1988**, *89*, 2257−2270.
(31) Yamamoto, T.; Nozaki, K.; Hara, T. *J. Chem. Phys.* **1990**, *92*, 631−641.
(32) Yeo, Y. H.; McGonigal, G. C.; Thomson, D. J. *Langmuir* **1993**, *9*, 649−651.
(33) Yoshimura, K.; Arakawa, H.; Ikai, A. *Jpn. J. Appl. Phys.* **1995**, *34*, 3368−3372.
(34) Takeuchi, H.; Kawauchi, S.; Ikai, A. *Jpn. J. Appl. Phys.* **1996**, *35*, 3754−3758.
(35) Smith, D. P. E.; Heckl, W. M.; Klagges, H. A. *Surf. Sci.* **1992**, *278*, 166−174.
(36) Strohmaier, R.; Ludwig, C.; Petersen, J.; Gompf, B.; Eisenmenger, W. *Surf. Sci.* **1994**, *318*, L1181−L1185.
(37) Fisher, A. J.; Blöchl, P. E. *Phys. Rev. Lett.* **1993**, *70*, 3263−3266.
(38) Groszek, A. J. *Nature* **1964**, *204*, 680.
(39) McGonigal, G. C.; Bernhardt, R. H.; Thomson, D. J. *Appl. Phys. Lett.* **1990**, *57*, 28−30.
(40) McGonigal, G. C.; Bernhardt, R. H.; Yeo, Y. H.; Thomson, D. J. *J. Vac. Sci. Technol. B* **1991**, *9*, 1107−1110.
(41) Rabe, J. P.; Buchholz, S. *Science* **1991**, *253*, 424−427.
(42) Ryckaert, J.-P.; Klein, M. L. *J. Chem. Phys.* **1986**, *85*, 1613−1620.
(43) Yamamoto, T. *J. Chem. Phys.* **1988**, *89*, 2356−2365.
(44) Fang, H.; Giancarlo, L. C.; Flynn, G. W. Submitted for publication.
(45) Faglioni, F.; Claypool, C. L.; Lewis, N. S.; Goddard, W. A. *J. Phys. Chem. B.* **1997**, *101*, 5996−6020.
(46) Eigler, D. M.; Weiss, P. S.; Schweizer, E. K.; Lang, N. D. *Phys. Rev. Lett.* **1991**, *66*, 1189−1192.
(47) McMenamin, J. C.; Spicer, W. E. *Phys. Rev. B* **1977**, *16*, 5474−5487.
(48) Mattheiss, F. *Phys. Rev. B* **1973**, *8*, 3719−3740.
(49) Coehoorn, R.; Haas, C.; Kijkstra, J.; Flipse, C. J. F.; deGroot, R. A.; Wold, A. *Phys. Rev. B* **1987**, *35*, 6195−6202.